Viability of coaxial atomization for disintegration of cell solutions in cell spray applications

Malte Bieber[*], Sarah Menzel[2], Anja Lena Thiebes[2], Christian Gabriel Cornelissen[2], Stefan Jockenhoevel[2], Reinhold Kneer[1], Manuel Armin Reddemann[1]
[1]Institute of Heat and Mass Transfer, RWTH Aachen University, Germany
[2]Department of Biohybrid & Medical Textiles (BioTex) at AME-Helmholtz Institute for Biomedical Engineering, ITA-Institut für Textiltechnik, RWTH Aachen University, Germany and at AMIBM-Masstricht University, The Netherlands
*Corresponding author: bieber@wsa.rwth-aachen.de

Abstract

Treating Leukemia with intravenous stem cell transplantation represents a well-established therapy technique. For applications, that require high local cell concentrations, transplantation by conventional intravenous injection is less potent, due to cell distribution with blood circulation. Instead, spraying them directly onto the injured or diseased area shows promising results in various applications, e.g. superficial treatment of topographically challenging wounds, in situ seeding of cells on implants, deposition of cells in tubular organs for stem cell therapy.
The present work aims for a basic knowledge about viability boundaries for coaxial cell-spray atomization and the reciprocal influence between cells in solution and primary breakup mechanics. A generic modular nozzle is developed, to ensures reproducible boundary conditions. Investigations are conducted regarding primary breakup and relations between resulting droplet size distribution and cell survival. Measurements are performed, utilizing microscopic high-speed visualization with suitable image post processing. Cell viability is analyzed using phase contrast microscopy prior and after atomization. A relation between Rayleigh-Taylor instability wavelength and droplet size distributions by means of Sauter mean diameter (SMD) and cell survival rate (CSR) is suggested. A power law is presented, exclusively dependent on dimensionless measures ($\lambda_\perp \sim \mathrm{Re}^{-1/2}\mathrm{We}^{-1/3}$) which is found to be proportional to SMD and CSR.

Keywords

cell spray, coaxial atomization, cell survival

Introduction

Stem cell therapy is a research field in regenerative medicine with increasing importance due to the ability of cells to support healing of afflicted tissue. A well-established example represents the treatment of Leukemia by means of intravenous stem cell transplantation, where cells distribute by blood circulation within the organism after injection. To utilize the full potential of stem cells for applications that require high local cell concentration, alternative approaches for transplantation would be desirable, that enable local treatment rather than homogeneous distribution. An example for the requirement of high concentrations is the treatment of Acute Lung Injury (ALI) or Acute Respiratory Distress Syndrome (ARDS), both resulting from inhalation of biological toxins or toxic chemicals [1]. Despite extensive research, the mortality rate remains high (40%) for both diagnoses [2]. As stated in [3], the anti-inflammatory properties of intrapulmonary instilled MSCs decrease the severity of endotoxin-induced ALI and improves survival in animal studies, though the increased liquid feed may further damage the lung tissue. Minimization of liquid feed into the lung could be achieved by using droplets as a carrier medium. A well-established technique for drug delivery in the lung using droplets, is the nebulization of liquids into a fine mist, that is directly inhaled. However, nebulization of cell solutions leads to high cell mortality rates [4]. In addition, direct inhalation is characterized by high deposition at the throat and at the first bifurcation, while in case of ALI/ARDS, the area of treatment is located at the alveolar regions. Therefore, the development of a suitable technique is required, that ensures high cell survival and reliable deposition at the area of treatment.

In this context, spraying of stem cells represents a promising approach. Suitability of cell spraying was already shown for external/superficial applications e.g. treatment of burn injuries by [5], treatment of topographically challenging wounds by [6] and most recently in [7]. However, application of cell-sprays within the human body was not realized so far. A flexible endoscopic spraying device was introduced by [8], enabling the atomization of therapeutic liquids and thus reliable local deposition of liquids in hollow organs. Utilized components are i) cell-thrombin-suspension and ii) fibrinogen, each dissolved in a tris-buffered-saline solution (TBS). Both solutions are injected through an endoscopic nozzle and are atomized by a coaxial air stream. After application, the fibrinogen polymerizes to fibrin gel, gluing the cells onto the area of treatment.

Cells in buffered solution are spherical and move with the surrounding fluid. However, they are prone to external forces, that possibly lead to destruction of cell membrane. Three destruction mechanisms for cell membranes have been investigated for syringe needle flow: cell deformation by pressure, linear shear flow and extensional flow origin from inlet flow conditions [9]. Pressure and shearing took minor roles in cell destruction, since spheres are generally pressure resistant and linear shearing causes them to spin within the surrounding fluid. Spinning reduces the stress applied on the cell membrane, due to circumferential distribution of the force application point [10]. However, while

not being the main cause of cell damage, shearing influences the function of cells after application, as it influences cell differentiation [11]. Contrary, extensional flow imposes a local force onto the cell, causes deformation and potentially destroys the membrane as shown for synthetic capsules [12]. Hence, extensional flow is assumed to be the main cause of membrane damage. Yet, in coaxial air assisted endoscopic atomization, all three destruction mechanisms are presumably relevant, as cells are first injected into the working channel, continue to flow through catheter and nozzle exit and until they are finally atomized via coaxial airflow. In addition, the atomization process itself is characterized by a combination of high shearing and extensional flows. The liquid phase ejects through the nozzle, where it is sheared and accelerated by the coaxial air stream. Transverse instabilities of the liquid jet grow in amplitude and eventually form ligaments [13]. Further acceleration of these ligaments results in extensional flow and possibly in cell damage. Nonetheless, viability of endoscopic cell spray has been shown with high survival rates of >90% [14] and a profound investigation of endoscopic cell spray has revealed no influence of the injection system on cell mortality [15].

In order to reach alveolar regions, directly inhaled particles need to be smaller than 10 µm in diameter [16]. Droplets generated with an endoscopic nozzle can be deposited directly into the lung airflow and bypass first bifurcations. Nevertheless, based on the findings of Heyder et al. [16] a high atomization level is necessary with droplet sizes in the range of cell diameter ($\sim$15 µm).

In this work, an overview is presented regarding the effect of high atomization on cell viability. In addition, the primary breakup at nozzle exit is investigated with respect to reciprocal influence between cells in solution and breakup mechanics.

Material and methods

Potential influence of cells in tris-buffered solution (TBS) on the atomization process and the resulting spray character is investigated in a series of spray experiments with cell suspension and pure TBS for reference. Therein, the mass gas-liquid-ratio (GLR) is varied and optical measurement techniques are utilized for data collection. The cell suspension is injected into the nozzle, atomized, recollected and analyzed with respect to cell survival rate. The analysis of the spray character in combination with cell survival measurements might lead to findings regarding a link between cell survival and droplet size distributions or atomization mechanics.

Injected substances:
Reference measurement without cells are performed using pure tris-buffered saline (TBS), prepared by dissolving 4.36 g Tris/HCL, 0.64 g Tris base, 8 g NaCl and 0.2 g KCl diluted to 1000 ml with H2O with pH value adjustment to 7.4 with HCl. For experiments including cells, TBS solution is enriched with living cells of A549 human cell line until a concentration of $1.6 \cdot 10^6$ cells/ml is achieved. Note, that cells in TBS are spherical with an average cell diameter of 15 µm, hence in the same order as mesenchymal stem cells, utilized in stem cell therapy [18]. Additionally, the selected cell concentration does not influence the fluid properties and is low enough for the fluid to be considered newtonian [17]. All substances are stored and injected at ambient conditions of T = 293.15 K and p = 100 kPa, thus fluid temperature matches ambient temperature with corresponding material properties (ρ = 1000 kg/m^3 and ν = $1.06 \cdot 10^{-6}$ m^2/s [15]).

Test setup for spray generation and analysis:
The general test setup is presented in Figure 1 (left). The spray, generated by coaxial atomization, is injected into a flow chamber with side windows for optical access. Visualization of the propagating spray is provided by a combination of high-speed shadowgraphy using incoherent pulsed light. The liquid mass flow can be adjusted through a linear translation stage, that is utilized to actuate the syringe. The gas volume flow rate is adjusted and monitored by a combination of valve and rotameter within a range of 0.5 m^3/h $\leq$ 6 m^3/h. A schematic of the generic coaxial nozzle is shown in Fig: 1 (right). It's geometry is based on previous works, in which endoscopic catheter nozzles have been utilized. Thus, the generic nozzle mimics catheter nozzle flow conditions but enables generic reproducible boundary conditions. Core of the nozzle is a straight tube with a connection possibility for sterile syringes at the top and small wall thickness (200 µm), to ensure a minimum gap between liquid and gas phase. This way, the interface boundary layer matches the gas boundary layer at nozzle exit, since the gap between liquid and gas phase is negligible. The tube is surrounded by an annular flow channel for coaxial atomization. The outer diameter of the annular flow channel is chosen to D = 3 mm and thus matches the working channel diameter of bronchoscopes.

The tube is exclusively attached to the upper body at the liquid inlet. The upper body is loosely connected to the lower body via three screws and tightened with 3 compression springs. This way, the upper body including the tube can be tilted relative to the lower body, which enables a precise coaxial and axial alignment of the tube relative to the annular air flow channel. The gas inlet is oriented perpendicular to the air flow channel, forcing the gas stream to turn directly into a flow straightener. From there on, the air flow enters an exchangeable nozzle tip, until it ejects parallel with the liquid flow.

Spray visualization:
To analyse the propagating spray, high-speed imaging (Fastcam SA-X, Photron Limited, 1024x1024) is utilized at 12,500 fps in combination with suitable image post processing. The qualitative spray character is determined via macroscopic imaging with a constant Xenon light source and Zeiss makro planar t* 2/100 mm zf camera lens, to monitor the general spray character and to define the ideal position for microscopic imaging. Microscopic imaging is performed to capture the primary breakup and droplet propagation, by using a monochromatic and incoherent
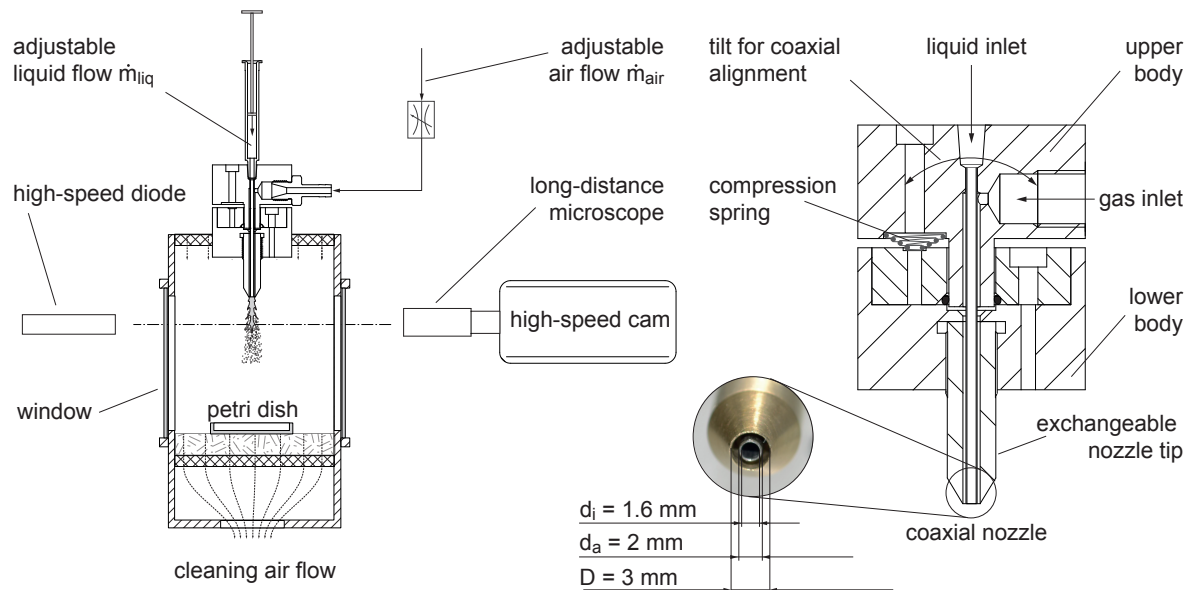
Figure 1. Left, experimental setup for spray investigation of coaxial gas stream driven atomization. Characterization of dispersed phase is done using macroscopic backlight visualization and long-distance transmitted light microscopy. Survival rates are determined before injection and after collection of droplets. Right, detailed presentation of modular coaxial nozzle design.

pulsed light source (Cavilux Smart, 640 nm wavelength, 10 ns pulse duration) and a Navitar Mag Zoom Lens with 12:1 zoom ratio set to 4.66 µm/pixel, resulting in a 4.8mm x 4.8mm frame size. Determination of resulting droplet diameters requires microscopic capturing sufficiently far from nozzle exit to ensure a fully atomized spray. Therefore, the investigated window ranges from 12 mm to 16.8 mm below nozzle exit. The typical spray cone angle for coaxial air assisted atomization is 20°[21]. To capture the entire spray, it is scanned horizontally in several high-speed videos, that are recombined afterwards in conducted image post processing. To investigate primary breakup, additional microscopic images are taken directly at nozzle exit with identical frame size.

Image post processing:
The image post-processing divides each high-speed video into individual images with a constant interframing time of 0.4 ms. This way, over-weighting of slow droplets (with minimal velocity of 12.5 m/s) by multiple detection in one frame is avoided. For each considered frame a binarized image is generated, suitable for detection and evaluation of coherent areas, representing droplets. Pixels of coherent areas are counted and the corresponding eccentricity, as well as the equivalent circle diameter evaluated, which is convertible into metric units. In two dimensional pictures overlapping droplets are treated as single droplets with high eccentricity. Droplets with high eccentricity have high potential for secondary droplet breakup and overlapping or high aspect ratio droplets are potential error sources for calculation of Sauter mean diameter (SMD). Droplets with eccentricity e > 0.7 are therefore not taken into account resulting in a maximum error potential caused by eccentricity of 5.77%.

To evaluate whether identified droplets are off focus or not, two distinct filter sets (with different gamma value, contrast and grey threshold) are applied. The sensitivity regarding intensity gradients differs for each filter leading to differing detected droplet sizes for out of focus droplets. This can be used for droplet selection, in order to consider exclusively in focus droplets. For more information see [15, 17].

Test parameter:
 The hydrodynamic entrance length is a function of characteristic length and Reynolds number. For laminar pipe

Table 1. Investigated parameter set for the gas flow with resulting mass gas-liquid-ratio (GLR), vorticity thickness δ and Weber number constructed on vorticity thickness

$\dot{V}_{gas}$	$\dot{m}_{gas}$	Re_{gas}	GLR	δ	We_{δ}
m^3/h	$10^{-3} \cdot$ kg/s	–	–	$10^{-5} \cdot$ m	–
1.39	1.17	6848	2.95	7.52	15.58
1.81	1.52	8879	3.82	6.77	23.01
2.28	1.92	11232	4.84	5.94	32.74
2.86	2.40	14036	6.04	5.28	45.74
3.53	2.97	17352	7.47	4.73	62.87
4.41	3.71	21687	9.34	3.8	87.84
6.07	5.11	29833	12.84	3.24	141.73

flow, it can be determined according to $L_h/d_i = 0.06 \cdot Re$ [20]. With a tube aspect ratio of $L/d_i = 37.5$ and liquid Reynolds number $Re_{liq} \leq 625$, a fully developed laminar velocity profile can be assumed at nozzle exit for every combination of parameter. The liquid Reynolds number for tube flow is calculated according to

$$Re_{liq} = \frac{4 \cdot \dot{m}_{liq}}{d_i \cdot \pi \cdot \eta_{liq}}. \tag{1}$$

The corresponding mass flow rate is determined by the syringe actuation velocity, density and the syringe diameter and adjusted to a resulting liquid Reynolds number $Re_{liq} = 300$. This way, the hydrodynamic entry length ($L_h/d_i = 18$) is reasonably smaller than the tube aspect ratio presented above.

The gas flow channel is characterized as an annular tube with a corresponding air Reynolds number

$$Re_{air} = \frac{u_{exit} \cdot 2 \cdot s}{\nu_{gas}} \tag{2}$$

where $s = (D - d_a)/2$ (see Figure 1) represents the gap size between tube and coaxial air flow channel. Air flow monitoring is performed through pressure corrected[*] rotameter measurement. In Tab. 1, the investigated parameter settings for the air flow are presented. The minimum gas volume flow rate is set, to always ensure a fully atomized jet. The massflow rate $\dot{m}_{gas}$ is calculated through the ideal gas law and velocity $u_{exit,gas}$ through continuity. The GLR is calculated according to $GLR = \dot{m}_{gas}/\dot{m}_{liq}$.

Determination of cell survival rates:

For determination of cell survival rates, the spray is collected in a Petri dish, recollected by pipetting, dyed with Trypan blue and finally analyzed using an Axiovert 40 C phase-contrast microscope with a Zeiss AxioCam ERc 5s. Thereby, the amount of living cells within a control area is determined and compared with the cell concentration of untreated cell suspension. The resulting sample size of cells varies around 300 detected cells in the control area. Two "positive controls" are evaluated: First, the cell survival rate in the original cell suspension pre injection and secondly the cell survival rate after surpassing the entire injection system including target impact but without air flow and thus without atomization. Comparing the cell survival rates before and after injection without airflow leads to conclusions about the influence of injection system as well as target impact on the cell survival rate. With knowledge of the original cell survival rate as well as the injection influence, exclusively the influence of the atomization process on the cells can be investigated through subtraction of critical side effects, e.g. extensional syringe flow, tube flow or target impact.

Primary breakup theory of coaxial atomization

The following brief description of theoretical background is based on the findings of Marmottant and Villermaux [13]. When the liquid jet emerges into a stationary atmosphere, capillary Plateau–Rayleigh instabilities are evolve. An additional axisymmetric destabilization occurs, when a coaxial gas flow is added, with an exit velocity $u_{exit,gas}$ significantly larger than the liquid exit velocity $u_{exit,liq}$ (see Figure 2). The acceleration of the interface in radial direction is oscillating, i.e. the local direction of acceleration alternates towards gas phase and liquid phase respectively. Pulsation of the surface waves can be expressed as $\omega_L = 2\pi \cdot (u_u - u_{liq})/\lambda \sim (\rho_{gas}/\rho_{liq})^{1/2} \cdot u_{gas}/\lambda$ with $\lambda \sim \delta (\rho_{liq}/\rho_{gas})^{1/2}$ representing the wavelength of the axial perturbation. A perpendicular acceleration ($g = a \cdot \omega_L^2 \cdot \sin(\omega t)$) can be determined including the wave amplitude a. While directing towards the liquid phase, this acceleration is unstable, causing transverse Rayleigh-Taylor instabilities, that are oriented in azimuthal direction (see Figure 2). As a consequence, instabilities cause indentations of the rim, ligament formation and finally disintegration into droplets.

The azimuthal perturbation wavelength ($\lambda_\perp$) depends on surface tension and is proportional to the undulation velocity u_u. For a plane surface, the temporal Rayleigh-Taylor growth rate is given as

Figure 2. Schematic of transvese and azimuthal instabilities

$$\omega_{i,RT} \sim \left(\frac{\rho_{liq} \cdot g^3}{\sigma} \right)^{\frac{1}{4}} \quad \text{and} \quad \lambda_{RT} \sim \left(\frac{\sigma}{\rho_{liq} \cdot g} \right)^{\frac{1}{2}}. \tag{6}$$

[*]The rotameter, calibrated for ambient pressure (p_{amb}) and monitoring the air flow, is located prior the coaxial nozzle. Thus, the static pressure inside the rotameter increases, due to pressure losses inside the nozzle and the measurement requires correction, regarding the resulting change of gas density. The measured flow-rate is based on force equilibrium between the weight force of the float body (index s) and aerodynamic force imposed by the gas (index g). Using continuity and with the assumption, that the density of the solid float body is significantly higher than the gas density, a proportionality relation of the flow-rate can be developed.

$$\dot{V} \sim \sqrt{\frac{(\rho_s - \rho_g) \cdot g \cdot V_s}{\rho_g}} \sim \sqrt{\frac{\rho_s}{\rho_g}} \tag{3}$$

With knowledge of the increased pressure the measured rotameter scale value can be corrected according to

$$\frac{\dot{V}_{meas}}{\dot{V}_{corr}} = \frac{\sqrt{\rho_s/\rho_{g,cal}}}{\sqrt{\rho_s/\rho_{g,real}}} = \sqrt{1 + \frac{p_{amb}}{p_{amb} + \Delta p}}. \tag{4}$$

The obtained volume flow rate is assigned to the increased pressure inside the rotameter. To evaluate the volume flow rate at the nozzle exit, further adjustment is necessary, that includes the expansion towards nozzle exit by utilizing the ideal gas law.

$$\dot{V}_{exit,nozzle} = \dot{V}_{meas} \cdot \sqrt{1 + \frac{p_{amb}}{p_{amb} + \Delta p}} \cdot \left(1 + \frac{p_{amb}}{p_{amb} + \Delta p} \right) = \dot{V}_{meas} \left(1 + \frac{p_{amb}}{p_{amb} + \Delta p} \right)^{\frac{3}{2}} \tag{5}$$
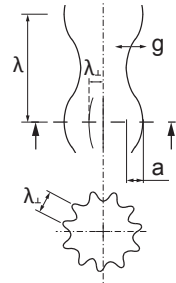
A critical condition for significant azimuthal instability development exists, when the inverse of the Rayleigh–Taylor growth rate is in the order of the transit time λ/u_u. In this case, a correlation between maximum acceleration of the interface (g_{max}) and selected wavelength (λ) and Weber number (We_λ) can be defined.

$$g_{max} \sim \left(\frac{\sigma}{\lambda \cdot We_\lambda^{-\frac{1}{3}}} \right)^2 \qquad \text{with} \qquad We_\lambda = \frac{\rho_{gas} \cdot u_{gas}^2}{\sigma/\lambda} \tag{7}$$

With $\lambda \sim (\rho_{liq}/\rho_{gas})^{(1/2)} \delta$ and a constant density ratio, the ligament spacing $\lambda_\perp$ can be expressed as a function of the vorticity thickness δ.

$$\lambda_\perp \sim \left(\frac{\sigma}{g_{max}} \right)^{\frac{1}{2}} \sim \delta \cdot We_\delta^{-\frac{1}{3}} \left(\frac{\rho_{gas}}{\rho_{liq}} \right)^{-\frac{1}{3}} \qquad \text{with} \qquad \delta \simeq 5.6 \cdot s \cdot Re_{gas,exit}^{-\frac{1}{2}} \qquad \Rightarrow \lambda_\perp \sim Re_{gas,exit}^{-\frac{1}{2}} \cdot We_\delta^{-\frac{1}{3}} \tag{8}$$

Ligament spacing is assumed to be directly proportional to resulting droplet size distributions, due to mutual correlation between ligament spacing, ligament diameter and resulting droplet sizes after ligament breakup. Ligament formation and potential extensional flows caused by ligament acceleration and thinning are assumed to be the main mechanic for cell damage [15]. Hence, maximum interface acceleration g_{max} is a potential measure for correlation between primary breakup and CSR and ligament spacing for resulting droplet size distributions of the spray.

Results and discussion

Investigation of mutual interaction between cells in solution and atomization is performed through variation of mass gas-liquid-ratio (GLR) in air assisted atomization of pure tris-buffered saline (TBS) and TBS enriched with living human cells. An overview is presented regarding jet breakup in air assisted atomization, followed by a brief discussion of resulting droplet size distributions, cell survival rates (CSR) and break up phenomena.

Primary breakup analysis
In Figure 3 four breakup regimes are presented. Left, a laminar jet exits the nozzle, that is perturbed in axial di-
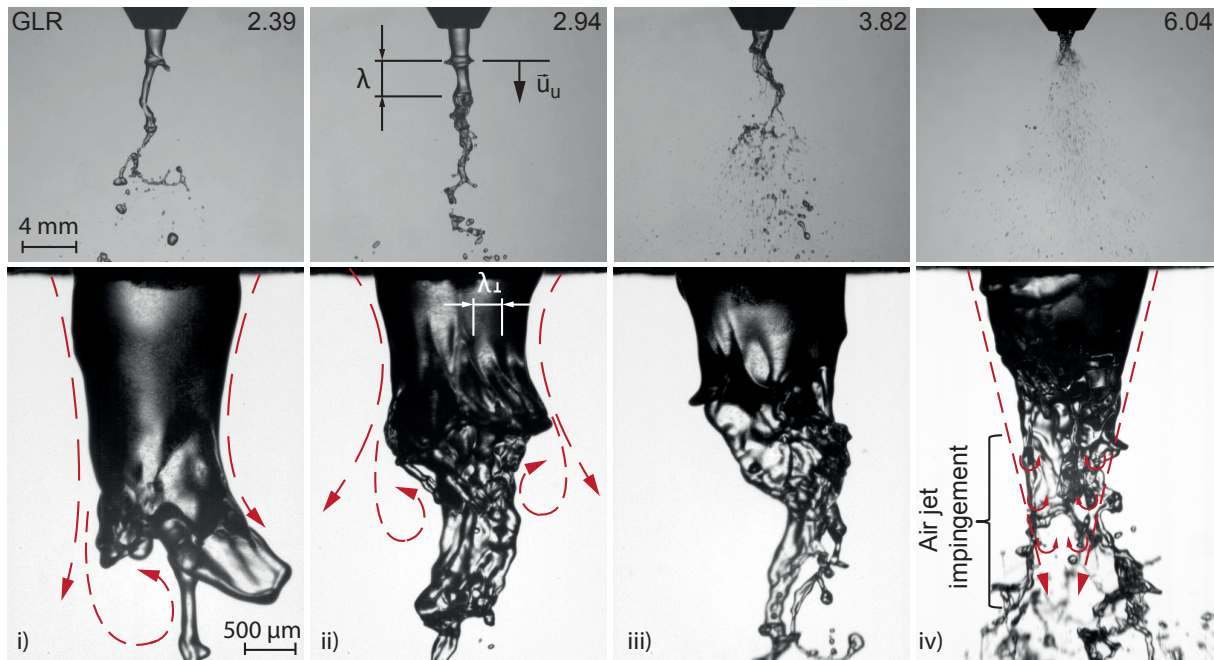

Figure 3. Macroscopic (top half) and microscopic (bottom half) images of the primary breakup of cell suspension are presented in dependency of the mass gas-liquid-ratio (GLR). Four different atomization regimes are shown; i) flapping: Axial modulation and high reciprocal flow interaction between gas and liquid face, ii) pulsing: Axial modulations superimposed by transverse Rayleigh-Taylor modulations and decreasing gas vortex sizes and liquid instability wavelengths, iii) transition: further decreasing flow characteristics, iv) disintegration: direct jet disintegration in the gas impingement region, liquid structures follow the gas flow.

rection (λ). Disintegration of the jet occurs exclusively at the tip. Interaction between liquid and gas phase causes the jet tip to flap, which eventually leads to jet breakup. The second case (GLR = 2.94) is characterized by axial pulsation of the jet, superimposed by transverse Rayleigh-Taylor instabilities ($\lambda_\perp$), causing ligament formation and jet breakup. This case is followed by a transition regime of decreasing perturbation wavelength $\lambda_\perp$. With further increasing GLR, the jet directly disintegrates in the air jet impingement region. Macroscopic perturbations are no longer visible and the liquid is directly dragged from a stationary liquid bulk, that is stabilized by the passing air flow. Primary breakup phenomena of the generic coaxial nozzle correspond well with the findings of Marmottant and Villermaux [13]. Hence, the gap thickness between gas and liquid phase is small enough to be negligible and

the nozzle enables reliable boundary conditions for experimental data comparison with the theoretical findings described above.

Droplet size distribution and cell survival

In flexible endoscopic cell spray applications, droplet size distributions, expressed by Sauter mean diameter (SMD), as well as CSR decrease exponentially with increasing GLR. Main difference between atomization of pure buffered solution (TBS) and atomization of cell suspensions (TBS+cells) have been found in the resulting SMDs for identical test settings [15]. Until today, there is no profound explanation for these results, since the material properties of cell suspension are identical to TBS and show strict newtonian behavior [17]. Even though, the correlation between increasing airflow (i.e. increasing hydrodynamic forces) and resulting cell damage are comprehensibly, but gathered without reproducible boundary conditions. In this work, a generic nozzle is utilized to guarantee reliable boundary conditions and test data. In Figure 4 droplet size distribution by means of SMDs are presented in dependency on Reynolds and Weber number, as well as corresponding CSRs. Reynolds and Weber power laws utilized on the
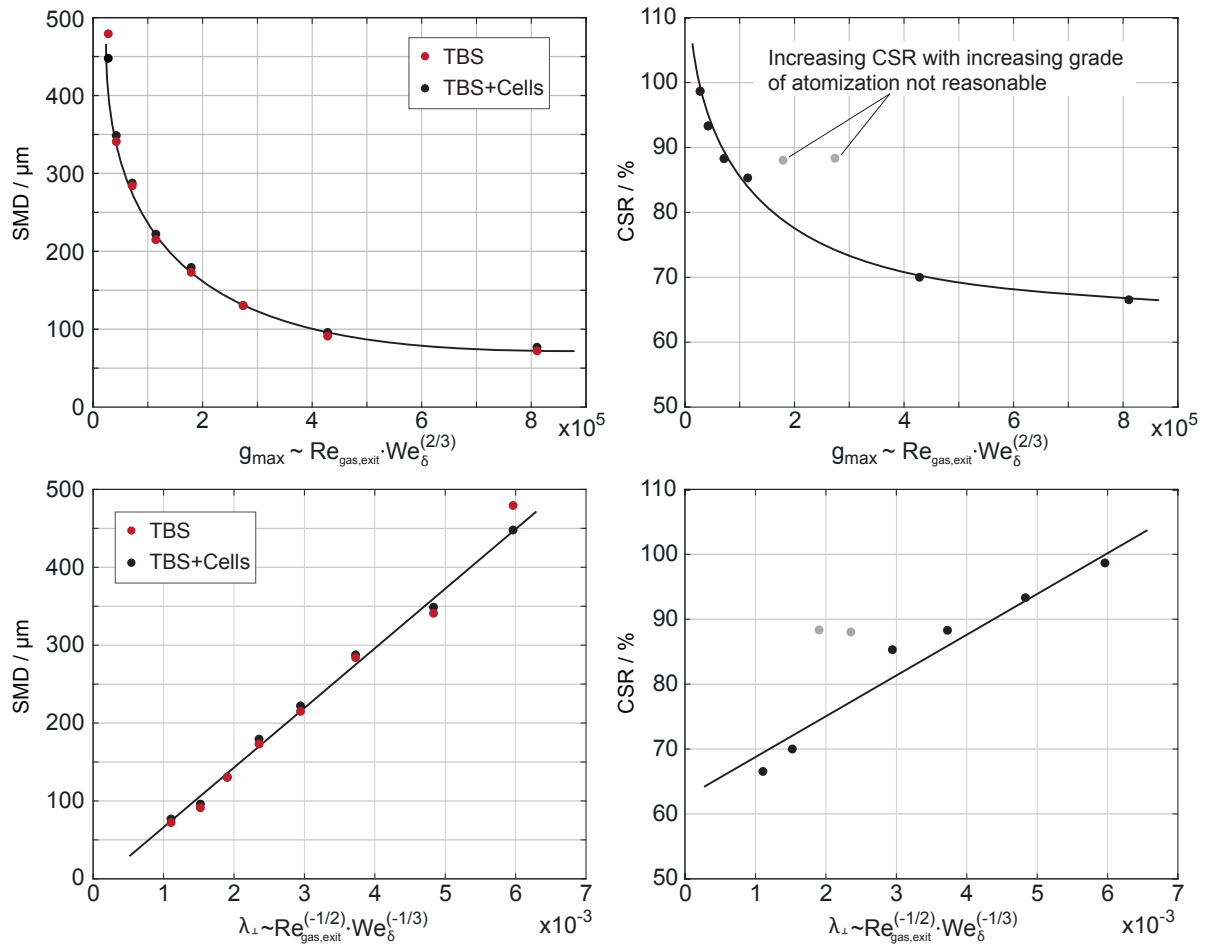

Figure 4. Left, droplet size distribution by means of Sauter mean diameter (SMD) is presented in dependency on Reynolds and Weber number. The Reynolds and Weber power law origins from Rayleigh-Taylor instability theory and is proportional to the maximum interface acceleration g_{max} (top) and transverse instability wavelength $\lambda_\perp$ (bottom). Right, the corresponding cell survival rates (CSR) are shown in dependency on equivalent dimensionless measures.

x-axis are developed from Rayleigh-Taylor instability theory and are proportional to the maximum interface acceleration g_{max} and transverse instability wavelength $\lambda_\perp$ (i.e. ligament spacing). The droplet size distribution decreases exponentially with increasing Reynolds and Weber number, hence with increasing air flow and interface acceleration. The cell survival rate reveals a similar behavior with a lowest CSR of 64.64 %. Note, that grey values in cell survival are not taken into account, as increasing CSRs assigned to higher grades of atomization contradicts earlier findings and presumably origin from statistical errors in CSR determination. The observation of increasing SMDs with cells added to the solution [15, 17] could not be reproduced and presumably origin in unreliable boundary conditions. This assumption is further supported by the finding, that the present cell concentration neither influences material properties nor newtonian behavior [17].

From (7) a proportionality between maximum interface velocity and ligament spacing can be determined.

$$\lambda_\perp \sim \left(\frac{1}{g_{max}}\right)^{\left(\frac{1}{2}\right)}$$

(9)

By adjusting the scaling of the abscissa accordingly, a linear dependency for SMD and CSR is found (see Figure 4, bottom half) exclusively dependent on dimensionless measures, that can be further utilized for development of a Reynolds and Weber power law and for prediction of SMD and CSR. Additionally, it represents a basis for future test series aiming for a deeper understanding of the main mechanics causing cell damage. Unlike assumed earlier, CSR is thus proportional to ligament spacing instead of maximum interface acceleration and should be in focus for future investigations regarding hydrodynamics and cell damage.

Particles in primary breakup

Microscopic investigation of primary breakup for GLR ≤ 3.82 is conducted regarding main breakup phenomena. Thereby, ligament and bag breakup of liquid sheets are found to be the dominant. In Figure 5, an exemplary propagating bag breakup and ligament formation of cell suspension is presented for GLR =3.82, captured at 20k frames per second. A liquid sheet evolves from the coherent jet, that is captured and thinned out by the coaxial air stream until it collapses. Part of the sheet disintegrates into droplets, while the rest recombines into a coherent ligament, driven by surface tension. The result is a circular coherent ligament, that further disintegrates into droplets by ligament breakup. At the beginning of sheet formation, black dots can be detected, that represent cells in the
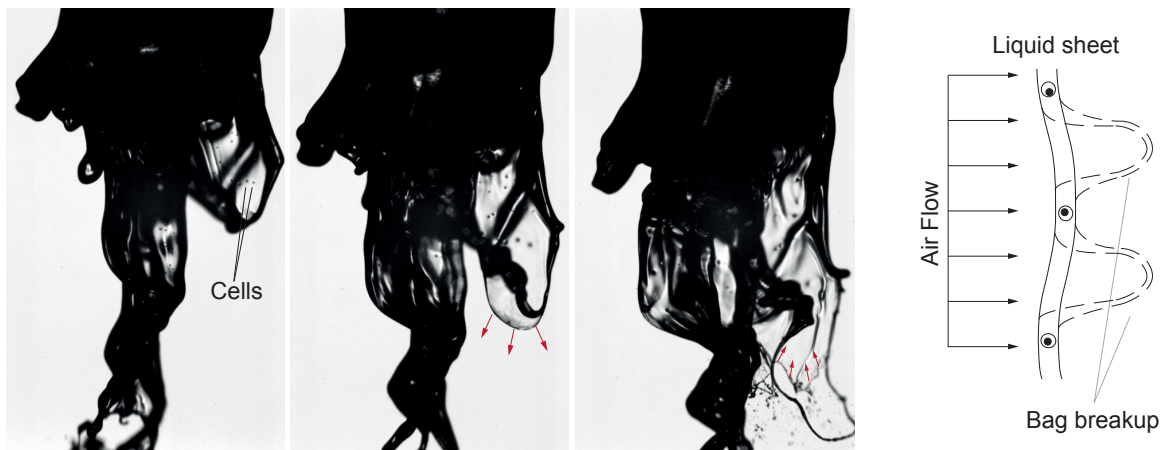

Figure 5. From left to right, propagating bag breakup and ligament formation of cell suspension is presented for GLR =3.82, captured at 20k frames per second. Black spots, visible exclusively in thicker parts of liquid sheets and ligaments, represent cells, that are surrounded by buffered solution. The lack of cells in thinning liquid sheets indicates, that the cells presumably act as a flow barrier/stabilizer. This way, the propagation of bag breakup happens favorably in regions with low cell concentration.

disintegrating jet. Note, that the exemplary images are representative for all bag breakups captured, and cells are exclusively located in thicker regions of the liquid sheet, rims or ligaments but rarely in further thinning regions, that are typical for bag breakup. The cells presumably act as a stabilizer and since the flow will always chose the path of least resistance, bag breakup is favorably located in areas with low cell concentration (see Figure 5, right). After breakup, a small mass fraction of the bag disintegrates into droplets, while the main fraction collapses and gathers into a coherent ring shapes ligament, including the cells. During atomization, cells are therefore most likely located in ligaments and not in liquid sheets. This phenomena supports the findings mentioned above, in which ligament formation and sizing directly correlates with cell survival rather then other breakup phenomena. Note, that this hypothesis requires further investigation with generic test setups and high particle concentration.

Conclusions

The present work represents a systematic investigation of a spray generated through coaxial air assisted atomization. The data is evaluated regarding primary breakup, droplet size distribution and the influence of atomization on cell survival. A series of spray experiments is conducted with varying mass gas-liquid-ratios (GLR) of air flow and cell suspension.

General phenomena of primary breakup are discussed in dependency of GLR and assigned to the context of Rayleigh-Taylor instability driven ligament formation. A relation between ligament spacing and droplet size distributions by means of Sauter mean diameter (SMD) and cell survival rate (CSR) is suggested, including a corresponding power law. The relation is exclusively dependent on dimensionless measures ($\lambda_\perp \sim \text{Re}^{-1/2}\text{We}^{-1/3}$) and found to be proportional to SMD and CSR.

Primary breakup in coaxial air assisted atomization is characterized by ligament and liquid sheet formation and breakup. Analysis of bag breakup reveals, that even though cells can be found in liquid sheets, evolving and thereby thinning areas of the sheet leading to bag breakup tend to lack presence of cells. The cells rather stay in thicker regions of the sheet, that are less influenced by the coaxial airflow. Therefore, the cells might act as a flow barrier and thereby stabilizing specific areas of high cell concentration. In this case airflow and liquid would always chose the path of least resistance and bypass the cells. The cells remain in ligaments, thus ligament formation and breakup are presumably the main phenomena influencing cell survival, which corresponds well to the proportional dependency of cell survival on ligament spacing.

References

[1] Angelini, D., Dorsey, R., Willis, K., Hong, C., Moyer, R., Oyler, J., Jensen, N., Salem, H., 2013, *Inhalation Toxicology*, 25(1), pp. 37–62.

[2] Lee, J., Gupta, N., Serikov, V., Matthay, M., 2009, *Expert opinion on biological therapy*, 9(10), pp. 1259–1270.

[3] Gupta, N., Su, X., Popov, B., Lee, J., Serikov, V., Matthay, M., 2007, *The Journal of Immunology*, 179, pp. 1855–1863.

[4] Sosnowski, T., Kurowska, A., Butruk, B., Jablczynska, K., 2013, *AIDIC Conference Series*, 11, pp. 371–380.

[5] Duncan, C., Shelton, R., Navsaria, H., Balderson, D., Papini, R., Barralet, J., 2005, *Journal of Biomedical Materials Research Part B: Applied Biomaterials*, 73(2), pp. 221–228.

[6] Gerlach, J. C., Johnen, C., McCoy, E., Bräautigam, K., Plettig, J., Corcos, A., 2011, *Burns*, 37(4), pp. e19–e23.

[7] Esteban-Vives, R., Choi, M., Young, M., Over, P., Ziembicki, J., Corcos, A., Gerlach, J., 2016, *Burns*, 42, pp. e99–e106.

[8] Thiebes, A. L., Reddemann, M. A., Palmer, J., Kneer, R., Jockenhoevel, S., Cornelissen, C. G., 2016, *Tissue Engineering Part C*, 22(4), pp. 322–331.

[9] Aguado, B., Mulyasasmita, W., Su, J., Lampe, K., Heilshorn, S., 2012, *Tissue Engineering Part A*, 18(7-8), pp. 806–815.

[10] Bluemink, J., Lohse, D., Prosperetti, A., and Wijngaarden, L., 2008, *Journal of Fluid Mechanics*, 600, pp. 201–233.

[11] Luo,W., Xiong,W., Zhou, J., Fang, Z., Chen,W., Fan, Y., Li, F.. 2011, *Acta biochimica at biophysica Sinica*, 43(3), pp. 210–216.

[12] Chang, K. and Olbricht, W. (1993). *Journal of Fluid Mechanics*, 250, pp. 587–608.

[13] Marmottant, P. and Villermaux, E. (2004). *Journal of fluid mechanics*, 498, pp. 73–111.

[14] Thiebes, A. L., Albers, S., Klopsch, C., Jockenhoevel, S.,Cornelissen, C. G., 2015, *BioResearch open access*, 4(1), pp. 278–287.

[15] Bieber, M., Thiebes, L.,Cornelissen, C.G., Jockenhoevel, S., Kneer, R., Reddemann, M.A., Sep. 5.-7. 2016, 27th European Conference on Liquid Atomization and Spray Systems, Brighton, UK.

[16] Heyder, J., Gebhart, J. Rudolf, G. Schiller, C.F. Stahlhofen, W., 1985, *Journal of Aerosol Science*,5, pp. 811–825.

[17] Bieber, M., Thiebes, L.,Cornelissen, C.G., Jockenhoevel, S., Kneer, R., Reddemann, M.A., 2017, *Atomization and Sprays, submitted*

[18] Ge, J., Guo, L., Wang, S., Zhang, Y., Cai, T., Zhao, R. C., Wu, Y., 2014, *Stem Cell Reviews and Reports*, 10(2), pp. 295-303.

[19] Gage, F. H., 1998, *Nature*, 392(6679), pp. 18–24.

[20] Kuemmel, W., 2007, "Technische Strömungsmechanik". B.G. Teubner Verlag.

[21] Wozniak, G., 2013, "Zerstäbungstechnik". Springer Verlag Berlin Heidelberg.